

Enhanced Method for Localization of Partial Discharges in Oil-Filled Transformers Using Acoustic Emission Signals

Yasutomo Otake¹, Kunihiko Tajiri²

^{1,2}*Mitsubishi Electric Co., Amagasaki, Hyogo, 661-8661, Japan*

Otake.Yasutomo@ce.MitsubishiElectric.co.jp

Tajiri.Kunihiko@ab.MitsubishiElectric.co.jp

ABSTRACT

Accurate measurement of partial discharges (PD) in power transformers is crucial for fault identification and effective maintenance planning. Acoustic emission (AE) sensing, less susceptible to external electromagnetic interference, offers non-invasive PD detection. This paper investigates the relationship between AE detection intensity, PD source type, and distance using AE sensors. Corona discharges exhibited the strongest AE wave intensities, followed by creepage discharges and PD in bubbles. AE wave intensity varies significantly based on discharge propagation speed, medium, and discharge space volume. The study experimentally compared three Time Difference of Arrival (TDOA) calculation methods for localization: energy criterion, Generalized Cross-Correlation (GCC), and GCC with Phase Transformation (PHAT). The energy criterion excelled in distributed sensor setups, while GCC-PHAT was superior in centralized configurations. GCC-PHAT, effectively suppressing noise and reflections, consistently outperformed standard GCC in accuracy, even at low discharge intensities. These findings promise improved precision and effectiveness in power transformer maintenance diagnostics.

1. INTRODUCTION

The electrical insulation of power equipment is crucial for safe and reliable power system operation. However, insulation degradation, accelerated by environmental factors, manufacturing defects, and stresses, can lead to partial discharge (PD) (CIGRE, 2015). PD, a localized insulation breakdown, intensifies over time, culminating in complete insulation failure (CIGRE, 2017). This results in significant economic losses and jeopardizes power system safety and stability. PD diagnostic testing is indispensable for preventing such incidents and enabling proactive maintenance planning. High-frequency current transformers,

ultra-high frequency (UHF) antennas, and acoustic emission (AE) sensors are employed for PD detection. AE sensing, immune to external electromagnetic interference, offers non-invasive PD detection in transformers.

Accurate detection and localization of partial discharges (PDs) are of paramount importance. Precise localization enables the identification of faulty components and facilitates efficient repair planning. Without PD localization, continued operation of a transformer is challenging, but with accurate localization, repairs can be targeted to the affected component, and combined with temperature history-based degradation diagnosis, continued operation may be possible.

AE sensors are widely used to identify PD sources by measuring the Time Difference of Arrival (TDOA) of AE waves at multiple sensors mounted on the transformer tank (Ghosh, Chatterjee & Dalai, 2017). TDOA refers to the difference in time it takes for a signal, such as an acoustic wave, to reach two or more sensors. Knowing the AE wave speed in transformer oil, the distance to the PD source can be calculated from TDOA. With four or more sensors, 3D PD localization is possible. Additionally, combined acoustic and electrical positioning systems (Markalous, Tenbohlen & Feser, 2008) utilize electrical PD detection alongside AE sensing.

AE signal waveforms are complex due to reflections, refractions, attenuations and diffraction within the transformer. This impacts TDOA accuracy and subsequent localization. The Generalized Cross-Correlation (GCC) method has been employed to enhance TDOA accuracy (Chen, Benesty & Huang, 2006).

Our study investigates a GCC-based TDOA approach for improved PD localization accuracy using AE sensors. We evaluate this method through oil-immersed PD tests, simulating real-world conditions. Our experiments cover both distributed and centralized sensor setups.

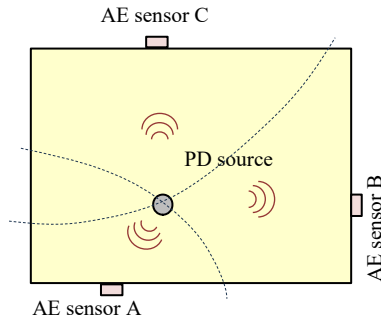
Yasutomo Otake et al. This is an open-access article distributed under the terms of the Creative Commons Attribution 3.0 United States License, which permits unrestricted use, distribution, and reproduction in any medium, provided the original author and source are credited.

<https://doi.org/10.36001/IJPHM.2024.v15i3.3852>

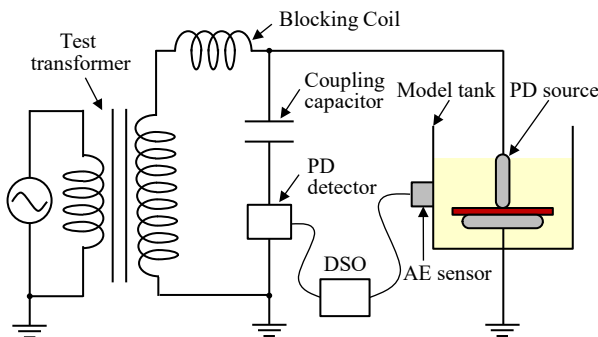
2. EXPERIMENTAL SETUP

Figure 1 illustrates the experimental setup for PD measurement in a simulated transformer model tank. The steel tank, with 400 mm sides and 3 mm thickness, was filled with mineral oil. Four AE sensors (Physical Acoustic, WD AH 17) were positioned on the tank's surface. AC voltage at 60 Hz generated PD, measured by a digital oscilloscope via a coupling capacitor and PD detection circuit. Simultaneously, AE sensors detected acoustic waves, amplified by 40 dB, and recorded on the digital oscilloscope at a 20 MS/s sampling rate.

Three PD sources were employed: protrusion corona, creepage discharge, and bubble PD. These PD types are representative of those commonly encountered in actual transformers (CIGRE, 2017). Table 1 details their specifications. Protrusion corona, simulating corona from metallic particles adhering to high-voltage conductors in real transformers, was generated using a 10 mm diameter electrode with a 10 μm tip radius and a 10 mm insulation gap. Creepage discharge, mimicking PD caused by coil support deterioration, was produced using a 10 mm diameter, 2 mm thick PB electrode. Bubble PD, resulting from dissolved air in oil, was induced between 10 cm diameter flat electrodes using a syringe.



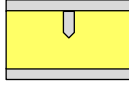
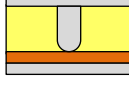
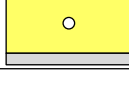
(a) PD source and AE sensor placement



(b) Test circuit

Figure 1. Experimental configuration.

Table 1. PD sources.

PD source	Image	Assumed event
Corona from protrusion		Metal particle in the oil adhere to the surface of H.V. conductor due to the electric field, causing a PD.
Creepage discharge		Deterioration of the insulating paper reduces the coil support. Discharge occurs due to proximity and high electric field between the charging section and the insulation paper.
PD in bubble		Dissolved air in the oil is attracted to high electric field points. Discharge occurs in the bubble.

3. EMISSION AND PROPAGATION OF AE WAVE

Figure 2 presents AE signal waveforms generated by a creepage discharge model. The figure compares signals from two sensors. AE sensor A, positioned 440 mm from the PD source, detects a signal 370 μs after the PD detector. Similarly, sensor B, 200 mm from the source, detects a signal 170 μs later. Calculating from these times, the AE wave propagation speed is determined to be 1.2 km/s. This value aligns with the typical range of 1.1 to 1.5 km/s for AE wave speed in oil, which varies based on oil temperature.

Figure 2 also reveals detected signal strengths of 13 mV for sensor A and 20 mV for sensor B. This signal strength varies with PD intensity, as illustrated in Figure 3. This figure correlates PD intensity with detection intensity for creepage discharges at distances of 150 mm, 300 mm, and 450 mm from the PD source. A clear trend shows that detection intensity decreases with increasing distance from the PD source.

Table 2 compares AE sensor sensitivity for different PD sources. Sensitivity was measured experimentally for each PD type at a standardized intensity of 100 pC.

For reference, detection sensitivity using UHF sensors, commonly used for partial discharge detection, is also included in Table 2 for comparison. Electromagnetic waves have a relatively strong correlation with PD charge quantity. On the other hand, acoustic emission waves have a weak correlation with PD charge quantity, which becomes more evident when compared with electromagnetic waves.

Corona discharges exhibit the highest AE wave intensity, followed by creepage discharges and bubble PD. The concentrated discharge space at the needle electrode tip enhances AE wave generation in corona discharges. Creepage discharges, with their wider, slower discharge spread, produce lower intensity waves. For bubble PD, the confined discharge space within the bubble limits AE wave intensity.

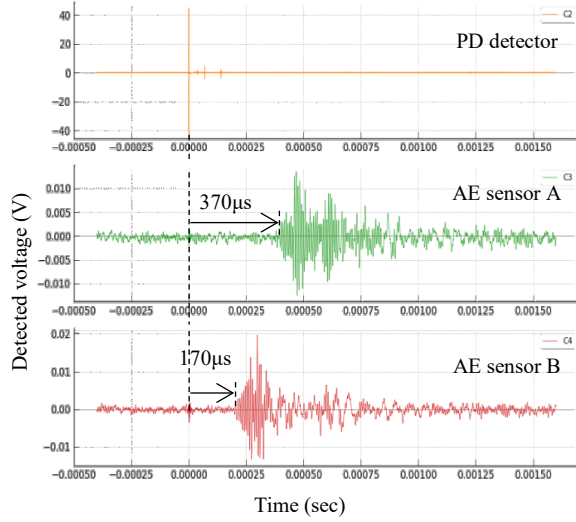


Figure 2. AE signal waveform (using the creepage discharge model).

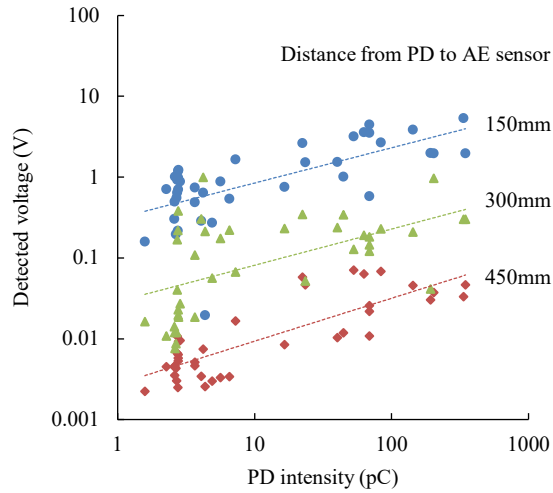


Figure 3. AE signal waveform (using the creepage discharge model).

Table 2. Comparison of Detection Sensitivity of Different PD sources and PD sensors.

PD Source	Corona from protrusion	Creepage discharge	PD in bubble
AE Sensors	1	0.54	0.23
UHF antenna	1	0.76	0.85

4. DENOISING METHOD

4.1. Time-frequency characteristics

External electromagnetic waves can interfere with AE sensors, compromising localization accuracy. To address this, we applied wavelet transform for noise reduction. Wavelet transform is a time-frequency analysis technique (Walnut, 2013) involving scaling and shifting a wavelet basis function, $\psi(t)$. Unlike the short-time Fourier transform, wavelets offer a balanced time-frequency resolution.

The wavelet transform of a signal, $v(t)$, is defined by equations (1) and (2), where the symbol * denotes complex conjugation, and scaling and shifting parameters are represented by a and b , respectively. Our study utilized the Gabor function as the wavelet basis, $\psi(t)$.

$$X(a, b) = \int_{-\infty}^{\infty} v(t) \psi_{a,b}^*(t) dt \quad (1)$$

$$\psi_{a,b}(t) = \frac{1}{\sqrt{a}} \psi\left(\frac{t-b}{a}\right) \quad (2)$$

Figure 4 presents time-frequency waveforms obtained through wavelet transform. Prior to PD-generated AE wave arrival, wideband oscillations are observed. Post-arrival, oscillations concentrate primarily within the 200-300 kHz range.

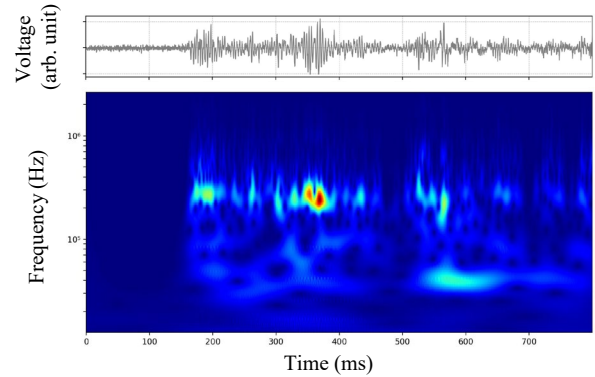


Figure 4. AE signal waveform (using the creepage discharge model).

4.2. Wavelet denoising

Noise reduction was achieved through the implementation of soft thresholding, utilizing a universal threshold calculated from the wavelet coefficients, $X(a, b)$, which were acquired using the wavelet transform (Zhong, Bi, Shu, Zhang & Li, 2021). Additionally, only the components within the AE sensors detection frequency band were employed, while the others were set to zero. Subsequently, an inverse wavelet transform was executed to transform the waveform back into a time domain waveform. Figure 5 shows the time domain waveforms before and after noise reduction, demonstrating the effective elimination of noise.

Noise reduction was achieved through soft thresholding of wavelet coefficients, $X(a,b)$, calculated using the wavelet transform ((Zhong, Bi, Shu, Zhang & Li, 2021). A universal threshold was determined from these coefficients. To isolate the signal within the AE sensor's detection band, components outside this range were nullified. An inverse wavelet transform then reconstructed the time-domain waveform. Figure 5 visually demonstrates the effectiveness of noise reduction by comparing waveforms before and after processing.

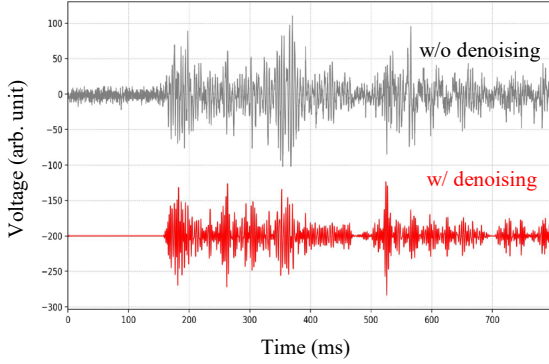


Figure 5. AE signal waveform (using the creepage discharge model).

5. LOCALIZATION METHOD BASED TDOA

An AE signal generated by PD is detected by sensors located at different positions. By calculating the TDOA of each sensor, the coordinates of the PD can be calculated using a geometric triangulation algorithm. In three-dimensional space, the TDOA of each sensor can be used with four or more AE sensors to construct the following non-linear equation. This equation can be solved numerically using the Newton-Raphson iteration method to calculate the discharge position (x, y, z) .

$$\begin{cases} \sqrt{(x-x_1)^2 + (y-y_1)^2 + (z-z_1)^2} = cT_1 \\ \sqrt{(x-x_2)^2 + (y-y_2)^2 + (z-z_2)^2} = c(T_1 + \tau_{12}) \\ \sqrt{(x-x_3)^2 + (y-y_3)^2 + (z-z_3)^2} = c(T_1 + \tau_{13}) \\ \sqrt{(x-x_4)^2 + (y-y_4)^2 + (z-z_4)^2} = c(T_1 + \tau_{14}) \end{cases} \quad (3)$$

where (x_i, y_i, z_i) are sensor coordinates, $i = 1, 2, 3, 4$, c is the AE wave velocity, T_1 is the signal arrival time of sensor 1, τ_{ij} is the time difference of the other sensors to sensor $i, j = 2, 3, 4$.

Localization error is calculated as:

$$e = \sqrt{(x_e - x_t)^2 + (y_e - y_t)^2 + (z_e - z_t)^2} \quad (4)$$

where (x_e, y_e, z_e) is the estimated value and (x_t, y_t, z_t) is the true value.

Considering that distance attenuation of signal strength affects localization accuracy, Root Mean Square Percentage Error (RMSPE) is used in this paper to assess errors.

RMPSE is a measure used in various fields to express prediction errors as a percentage of actual values.

It is calculated as follows:

1. Determine percentage error for each coordinate axis (x, y, z) using:

$$\begin{aligned} e_x &= \left| \frac{x_e - x_t}{x_t} \right| \times 100 \\ e_y &= \left| \frac{y_e - y_t}{y_t} \right| \times 100 \\ e_z &= \left| \frac{z_e - z_t}{z_t} \right| \times 100 \end{aligned} \quad (5)$$

2. Calculate the average percentage error across all axes.
3. Compute RMSPE as the root mean square of these average percentage errors over all observation points:

$$RMPSE = \sqrt{\frac{1}{n} \sum e_x^2 + e_y^2 + e_z^2} \quad (6)$$

5.1. Calculation of TDOA using Energy Criterion Method

Acoustic signals propagate by reflection, because the interior of power transformers contains structures such as windings and insulating paper. Therefore, AE sensors are reached by reflected waves via multiple paths in addition to direct waves. However, only the difference in arrival time through the direct path from the PD source to the multiple receivers is used for positional targeting. Other components caused by reverberation need to be excluded as noise. The energy criterion method is used to calculate the time of arrival of the AE wave for each sensor; using $S(t)$ as an indicator, the time at which the minimum value is obtained is determined by the formula below (Markalous et al, 2008).

$$S(t) = \sum_{i=1}^t v_i^2 - t\delta \quad (7)$$

$$\delta = \frac{\sum_{i=1}^t v_i^2}{N} \quad (8)$$

In this equation, v_i represents the detected voltage, and N represents the number of samplings. The first term on the right side of equation (7) is the cumulative energy obtained by integrating the squared detected voltage up to any time t . The second term is the sum of the cumulative energy over the entire region, as shown in equation (8), and averaged over the region, denoted as δ . The difference between these terms yields $S(t)$. The time t at which $S(t)$ attains its global minimum represents the time of arrival of the AE wave at the sensor. The TDOA can be obtained from the difference in the calculated times of arrival of the AE waves for each sensor.

5.2. Calculation of TDOA using GCC method

One method to suppress the effects of reverberation is the TDOA calculation method using the GCC function (Chaogeti, G. et al, 2018). $x_i(t)$ and $x_j(t)$ are the time waveforms of these sensors. $X_i(\omega)$ and $X_j(\omega)$ are the coefficients obtained by the short-time Fourier transform. The symbol $[\ast]$ denotes conjugation. The GCC function of the signals of these sensors is expressed as equation (9). This is a coupled operation in the time domain, where the output is zero at frequencies where the components are different for these sensors; $\Psi_{ij}(\omega)$ corresponds to a frequency filter, here a BPF centered at 100 kHz where the detected components are large.

$$R(\tau_{ij}(r_s)) = \frac{1}{2\pi} \int_{-\infty}^{\infty} \psi_{mn}(\omega) X_i X_j^*(\omega) e^{j\omega\tau} d\omega \quad (9)$$

$\tau_{ij}(r_s)$ quantifies the TDOA between acoustic waves from the same source propagating to these sensors along the shortest path, respectively. According to the definition, it is described as follows:

$$\tau_{ij}(r_s) = \frac{(\|r_s - r_i\| - \|r_s - r_j\|)}{v} \quad (10)$$

where r_s is the positions of the PD source and r_i and r_j are the positions of these sensors, v is the propagation velocity of AE wave. The maximum likelihood estimation of position r_s is described as follows:

$$r_s = \operatorname{argmax}_{r_s} \left(\sum_i^M \sum_{j=i+1}^M R(\tau_{ij}(r_s)) \right) \quad (11)$$

where the summation is over all sensor pairs (i, j) .

5.3. Calculation of TDOA using GCC-PHAT method

The Generalized Cross-Correlation with Phase Transform (GCC-PHAT) is a widely used technique in the field of signal processing for sound source localization (Knapp, C. et al, 1976). The essence of PHAT weighting is to normalize this cross-spectral density by its magnitude to emphasize phase information while mitigating the effect of signal amplitude. This is expressed as follows:

$$R'(\tau_{ij}(r_s)) = \frac{1}{2\pi} \int_{-\infty}^{\infty} \psi_{mn}(\omega) \frac{X_i X_j^*(\omega)}{|X_i X_j^*(\omega)|} e^{j\omega\tau} d\omega \quad (12)$$

The maximum likelihood estimation of position r_s is described as follows:

$$r_s = \operatorname{argmax}_{r_s} \left(\sum_i^M \sum_{j=i+1}^M R'(\tau_{ij}(r_s)) \right)$$

Using the r_s obtained from equation (13), $\tau_{ij}(r_s)$ can be calculated using equation (10), which represents the TDOA. This method is robust against noise and reverberation, making it highly effective for sound source localization in practical environments.

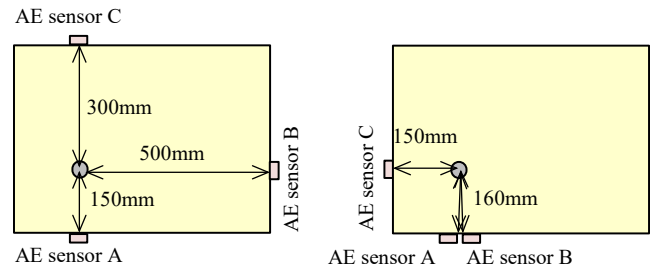
5.4. Comparison of Calculation Methods of TDOA

An experimental comparison of three TDOA calculation methods was conducted under distributed and centralized sensor configurations, as shown in Figure 6. Distributed placement involved sensors around the oil tank, while centralized placement focused sensors in one corner. A protrusion corona PD source, ranging from 100 to 1000 pC, was used for 100 discharges per configuration.

Figure 7 presents the results. The bar graphs represent the mean values, and the error bars indicate the 95% confidence intervals calculated using a t-test. A Welch's t-test was conducted to compare the energy criterion method with the GCC-PHAT method under denoising conditions. The results showed that the p-value was 0.021 for the distributed sensor configuration and 0.0092 for the centralized sensor configuration. Therefore, at a significance level of 5%, the energy criterion method outperformed for distributed sensor configurations, while the GCC-PHAT method exhibited superior performance for centralized sensor configurations. The energy criterion, though less precise, offered stable signal detection timings. The GCC method provided detailed TDOA calculations but was susceptible to attenuation and reflection issues at varying sensor distances. The GCC-PHAT method, effectively suppressing noise and reflections, outperformed standard GCC in accuracy.

It is concluded that the energy criterion is optimal for distributed sensor configurations, while GCC-PHAT excels in centralized setups. With denoising conditions, the appropriate selection of a TDOA calculation method can enhance PD source localization accuracy by 25% to 50%. These findings contribute to enhancing maintenance diagnostic accuracy. With compensation for the varying acoustic wave velocity due to oil type and temperature, these results can be extended to transformers with various insulating oils and molded transformers.

The development of algorithms that consider the structural complexity of wave propagation in transformers and the establishment of a robust methodology for selecting TDOA calculation techniques are identified as future research directions.



(a) Distributed placement (b) Centralized placement
Figure 6. Experimental Configuration.

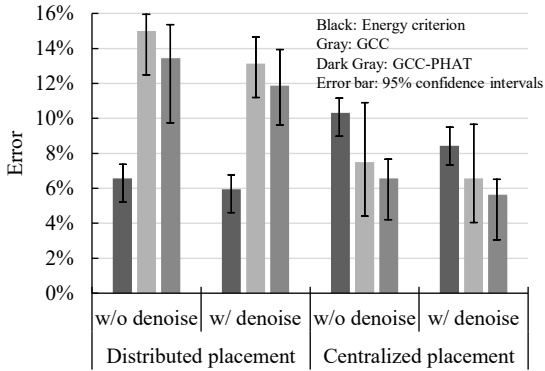


Figure 7. Experimental Result of Comparison of Calculation Methods of TDOA.

6. CONCLUSION

Accurate measurement of partial discharges (PDs) is crucial for ensuring the reliable operation of power transformers. By employing acoustic emission (AE) sensors, we examine the correlation between detection intensity, PD source type, and distance to the discharge origin. Results indicate that corona discharges generate relatively strong AE signals, enhancing their detectability. We compare three time-difference-of-arrival (TDOA) calculation methods: energy criterion, generalized cross-correlation (GCC), and GCC-PHAT. The energy criterion method proves most effective for sensors encircling the tank, while GCC-PHAT excels in centralized sensor configurations. Although the GCC method provides detailed calculations, its accuracy is compromised by waveform attenuation and reflections influenced by sensor-to-PD source distance. Conversely, GCC-PHAT effectively mitigates noise and reflection effects, consistently surpassing standard GCC in accuracy. These findings contribute significantly to improving the precision and reliability of maintenance diagnostics for power transformers.

REFERENCES

- Brochure, CIGRE. (2015) *642: Transformer reliability survey*: Final report of working group A2-37.
- Brochure, CIGRE (2017) *676: Partial Discharges in Transformers*: Final report of working Group D1-29.
- Hussain, M. R., Refaat, S. S., & Abu-Rub, H. (2021). Overview and partial discharge analysis of power transformers: *A literature review. IEEE Access*, 9, 64587-64605.
- Ghosh, R., Chatterjee, B., & Dalai, S. (2017). A method for the localization of partial discharge sources using partial discharge pulse information from acoustic emissions. *IEEE Transactions on Dielectrics and Electrical Insulation*, 24(1), 237-245.
- Markalous, S. M., Tenbohlen, S., & Feser, K. (2008). Detection and location of partial discharges in power transformers using acoustic and electromagnetic signals. *IEEE Transactions on Dielectrics and Electrical Insulation*, 15(6), 1576-1583.
- Chen, J., Benesty, J., & Huang, Y. (2006). Time delay estimation in room acoustic environments: An overview. *EURASIP Journal on Advances in Signal Processing*, 2006, 1-19.
- Gillette, M. and Silverman, H., (2008). A Linear Closed-Form Algorithm for Source Localization From Time-Difference of Arrival, *IEEE Signal Processing Letters*, vol. 15, pp. 1-4, doi: 10.1109/LSP.2007.910324..
- Mirzaei, H., Akbari, A., Gackenbach, E., Zanjani, M., and Miralikhani, K., (2013) "A Novel Method for Ultra-High Frequency Partial Discharge Localization in Power Transformers Using Particle Swarm Optimization Algorithm, *IEEE Electrical Magazine*, vol. 29, no. 2, pp. 26-39, doi: 10.1109/MEI.2013.6457597..
- Walnut, D. F. (2013). An introduction to wavelet analysis. *Springer Science & Business Media*, doi: 10.1007/978-1-4612-0001-7
- Zhong, J., Bi, X., Shu, Q., Zhang, D., & Li, X. (2021). An improved wavelet spectrum segmentation algorithm based on spectral kurtogram for denoising partial discharge signals. *IEEE Transactions on Instrumentation and Measurement*, 70, 1-8.
- Gao, C., Wang, W., Song, S., Wang, S., Yu, L., & Wang, Y. (2018). Localization of partial discharge in transformer oil using Fabry-Pérot optical fiber sensor array. *IEEE Transactions on Dielectrics and Electrical Insulation*, 25(6), 2279-2286.
- Knapp, C., & Carter, G. (1976). The generalized correlation method for estimation of time delay. *IEEE transactions on acoustics, speech, and signal processing*, 24(4), 320-327.
- Yasutomo Otake** was received the B.Sc. and M.Sc. degrees from Nagoya University in Japan in 2012 and 2014, respectively. He joined Mitsubishi Electric Corporation in 2014. Presently, he is a researcher at the Advanced Technology R&D Center and is mainly engaged in research on insulation technology of high voltage apparatus, such as power transformers, turbine generators and switchgears.
- Kunihiko Tajiri** was received the Ph.D. degree from the Osaka University, Japan in 2012. Presently, he is a group manager of Electrical Insulation Technology Group at Advanced Technology R&D center, Mitsubishi Electric Corporation. He has been involved with insulation engineering of power electronics devices.